THE JOURNAL OF PHYSICAL CHEMISTRY B
A JOURNAL OF THE AMERICAN CHEMICAL SOCIETY

pubs.acs.org/JPCB

Article

Influence of Internal Bond Rotation on Ultrafast IR Anisotropy Measurements and the Internal Rotational Potential

Published as part of The Journal of Physical Chemistry B virtual special issue "Gregory A. Voth Festschrift".

Aaron P. Charnay,[†] Junkun Pan,[†] and Michael D. Fayer*

Cite This: *J. Phys. Chem. B* 2024, 128, 280−286

Read Online

ACCESS | Metrics & More | Article Recommendations | Supporting Information

ABSTRACT: Measurement of molecular orientation relaxation using ultrafast infrared (IR) pump−probe experiments is widely used to understand the properties of liquids and other systems. In the simplest situation, the anisotropy decay is a single exponential reflecting diffusive orientational relaxation. However, the anisotropy decay is frequently biexponential. The faster component is caused by solvent caging restricting angular sampling until constraint release permits all angles to be sampled. Here, we describe another mechanism that limits the range of sampling, i.e., sampling of a restricted range of angles via internal bond reorientation on a rotational potential surface with barriers. If the internal angular sampling occurs faster than the entire molecule's diffusive orientational relaxation, it will produce a fast component of anisotropy decay with a cone angle determined by the shape of the internal rotation potential. We studied four molecules to illustrate the effects of internal bond rotations on anisotropy decay. The molecules are *p*-chlorobenzonitrile, phenylselenocyanate, phenylthiocyanate, and 2-nitrophenylselenocyante in the solvent *N*,*N*-dimethylformamide. The CN stretch is used as the IR chromophore. *p*-Chlorobenzonitrile does not have internal rotation; its anisotropy decays as a single exponential. The other three have bent geometries and internal rotation of the moieties containing the CN occurs; the anisotropies decay as biexponentials. The faster of the two decays can be understood in terms of motions on the rotational potential surface. A method is developed for extracting the intramolecular rotational potential surface by employing a modification of the harmonic cone model, and the results are compared to density functional theory calculations.

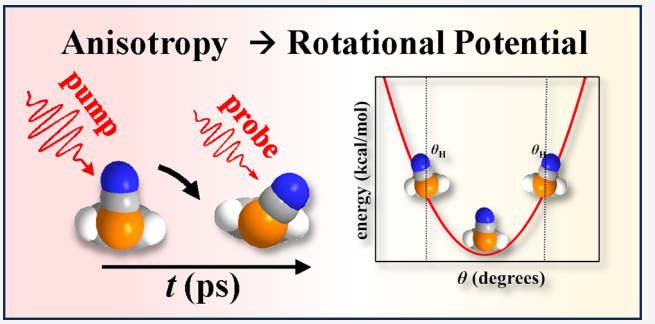

1. INTRODUCTION

Molecular reorientation is a subject with a long history and theoretical explication beginning with the Stokes−Einstein−Debye (SED) relation for rotational diffusion.[1,2] Molecular reorientation has been studied experimentally for decades.[3−5] One method in particular, infrared polarization-selective pump−probe spectroscopy (IR-PSPP), enables the quantification of molecular reorientation on ultrafast time scales by measuring the decay of the orientational anisotropy. The anisotropy decay measured by a PSPP experiment gives the second Legendre polynomial transition dipole time correlation function. For orientational relaxation that obeys the SED relation, the correlation function and the measured anisotropy will decay as a single exponential as the IR probe molecule undergoes rotational diffusion. Modifications of the SED equation using factors that account for the shape and hydrodynamic boundary condition of the probe molecule are frequently used.[6,7]

It is common to have a small IR probe molecule in a complex solvent, such as room-temperature ionic liquids (RTILs), concentrated salt solutions, and battery electrolytes in which the solvent forms a cage around the probe that lasts for a significant length of time.[8−10] In this situation, the probe's orientation relaxation is restricted for the cage lifetime. The probe can undergo orientational relaxation, but only over a limited range of angles, frequently described as a cone of angles or simply the cone. On the cage lifetime, the orientational constraint on the probe's angular sampling is released, and the probe can undergo full orientational relaxation, that is, sample all angles. In this situation, the anisotropy, $r(t)$, decays as biexponential. The first time constant is related to the time for the probe to sample the cone of angles, and the second time constant is the complete diffusive orientational relaxation.[11] The theory for the restricted orientational relaxation, called wobbling-in-a-cone (WIAC), was first developed in the 1970s and 1980s in the context of fluorescence depolarization and

Received: October 25, 2023
Revised: December 1, 2023
Accepted: December 6, 2023
Published: December 27, 2023

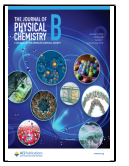

NMR experiments.[12−15] In IR experiments, it has been observed that there may be two levels of constraint release, which gives rise to two angular cones and a triexponential anisotropy decay.[16] In addition, there is a very fast, tens of femtoseconds, inertial component, which produces an inertial cone. All such components can be described in terms of the WIAC model.[17]

In this paper, we describe another mechanism that can give rise to biexponential IR-PSPP anisotropy decays. The mechanism involves internal bond rotation about the moiety of the probe molecule that contains the IR mode used to make the measurements. In the experiments presented below, we use the CN stretch of several molecules in the low-viscosity solvent, *N*,*N*-dimethylformamide (DMF). The four probe molecules are *p*-chlorobenzonitrile (pClBZN), 2-nitrophenylselenocyanate (2NPhSeCN), phenylselenocyanate (PhSeCN), or phenylthiocyanate (PhSCN). pClBZN does not have internal bond rotation that changes the orientation of the CN group. The anisotropy data from pClBZN in DMF is a single exponential decay. The other three molecules differ from pClBZN in that they have a bend at the chalcogen. This bent geometry introduces an interior degree of rotational freedom that can change the orientation of the CN. These three molecules in DMF have biexponential anisotropy decays.

The initial faster decay samples a limited range of angles as a result of internal bond rotation that is limited by the bond rotation potential energy surface. The data can be analyzed with the WIAC model, although the mechanism is distinct from the usual angular restrictions caused by intermolecular caging. The three chalcogen-containing molecules have different rotational potential surfaces with different barrier heights. Restricted rotation of the CN-containing groups on the different potential surfaces gives rise to different cone angles. We analyze the cone angles obtained from the experiments using a modified version of the harmonic cone theory.[18] This theory has been used to analyze restricted angular sampling caused by intermolecular caging as motions on a two-dimensional parabolic potential.[19,20] The theory is recast for a one-dimensional parabolic potential appropriate for the internal bond rotation. It is shown that information on the rotational potential surface can be obtained from the experimental anisotropy results. The harmonic potentials obtained from the analysis of the experimental cone data are compared to calculations using density functional theory (DFT) at the B3LYP level of theory with the 6-311++G(d,p) basis set in an implicit DMF solvent.

2. METHODS

2.1. Sample Preparation. Samples were prepared by dissolving an appropriate amount of probe molecule in *N*,*N*-dimethylformamide (DMF) to obtain a concentration of 250 mM. Samples were placed between two CaF_2 windows with a 250 μm spacer in an aluminum sample cell. The same sample preparation was used for FT-IR and ultrafast measurements.

2.2. FT-IR Measurements. FT-IR measurements for all samples were performed using a Thermo Fisher iS50 infrared spectrometer with a resolution of 0.24 cm^{-1}.

2.3. Ultrafast Infrared Measurement. A detailed description of the ultrafast IR pulse shaping system used in this study has been published previously.[16,21] In summary, a regenerative amplifier seeded by a Ti:sapphire oscillator was used to generate 800 nm pulses at a 3 kHz repetition rate with ∼80 fs pulse durations and 2 mJ per pulse. Using a home-built optical parametric amplifier, the 800 nm pulses are converted to ∼4.6 μm pulses with energies of 30 μJ. These pulses are chirp-corrected and near transform-limited. The IR pulse is tuned to the resonant frequency of the nitrile stretch of the probe molecule being studied. The pulse is then split into a strong pump (90% intensity) and a weak probe (5% intensity). The pump passes through a germanium acousto-optic modulator pulse shaping system. The pulse shaper is used to generate a four-shot phase cycle that reduces scattered light. In addition, it changes the frequency composition of every other pulse in a manner that greatly reduces spurious signals that result from solvent heating.[22]

The probe beam is delayed by a mechanical delay stage with a maximum delay of ∼1.7 ns. Immediately before the sample, a half-wave plate and polarizer are used to rotate the polarization of the pump beam to +45°. Immediately after the sample, a polarizer on a computer-controlled rotation stage is used to alternate between +45° (parallel) and −45° (perpendicular) to resolve the intensity of the transmitted probe beam that is either parallel ($I_{\parallel}$) or perpendicular ($I_{\perp}$) to the pump beam. An additional polarizer is placed after the rotating polarizer to ensure that the parallel and perpendicular transmitted probes have identical amplitude spectra after passing through a spectrograph and being detected by a 32-pixel mercury cadmium telluride array detector.

The parallel and perpendicular signals, $I_{\parallel}$ and $I_{\perp}$, can be combined according to eq 1 to obtain the isotropic signal, which is the population decays (vibrational lifetimes) of the CN stretch of the probe molecules, or with eq 2 to obtain the anisotropy decays (orientational relaxation):[23,24]

$$P(t) = (I_{\parallel}(t) + 2I_{\perp}(t))/3 \tag{1}$$

$$r(t) = \frac{I_{\parallel}(t) - I_{\perp}(t)}{I_{\parallel}(t) + 2I_{\perp}(t)} = 0.4C_2(t) \tag{2}$$

$C_2(t)$ is the second Legendre polynomial transition dipole orientational time correlation function.

2.4. DFT Calculations. Geometry optimization of phenylselenocyanate (PhSeCN), phenylthiocyanate (PhSCN), and 2-nitrophenylselenocyanate (2NPhSeCN) was performed using the Gaussian 16 quantum chemistry package at the B3LYP/6-311++G(d,p) level of theory to determine the bond lengths and distances between different atoms to calculate moments of inertia. Self-consistent reaction field was used with solvent specified as *N*,*N*-dimethylformamide. Potential energy surface scans were performed for PhSeCN, PhSCN, and 2NPhSeCN at the same level of theory for the dihedral C(Ph)−C(Ph)−Se/S−C(CN) from −90 to 90° with a step size of 5° to determine internal rotation potentials and barrier heights.

3. RESULTS AND DISCUSSION

3.1. Linear Absorption Spectra. Figure 1 shows the CN stretch absorption spectra of the four probes in DMF (solid curves). The baseline was subtracted from each spectrum using the spectrum of pure DMF. The resulting normalized spectra were fit to Voigt line shape functions (dashed curves). The centers and full widths at half-maximum are given in Table 1. The CN stretches of the three chalcogenides have very similar center frequencies, while the ClBZN is shifted to a higher frequency by ∼80 cm^{-1}. (Note the break in the horizontal axis in Figure 1.) The lower frequencies of the chalcogenides compared to ClBZN are caused by the decoupling of the CN

https://doi.org/10.1021/acs.jpcb.3c07080
J. Phys. Chem. B 2024, 128, 280−286

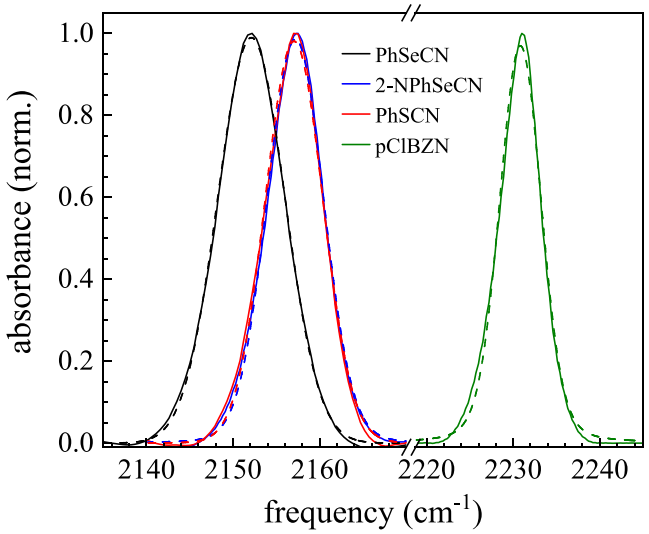

Figure 1. Linear FT-IR spectra of the CN stretch for the four probe molecules, phenylselenocyanate (black), 2-nitrophenylselenocyanate (blue), phenythiocyanate (red), and *p*-chlorobenzonitrile (green). The solid lines are the experimental data, and the dashed lines are fits to Voigt line shapes.

Table 1. CN Stretch Absorption Spectrum Parameters for the Four Probe Molecules

probe	center (cm^{-1})	fwhm (cm^{-1})[a]
PhSeCN	2152.11 ± 0.02	9.13 ± 0.06
2NPhSeCN	2157.19 ± 0.02	7.68 ± 0.04
PhSCN	2157.03 ± 0.02	7.85 ± 0.06
pClBZN	2230.81 ± 0.02	5.80 ± 0.05

[a]Full width at half-maximum amplitude of the absorption spectrum.

mode from the ring modes by the chalcogen. This decoupling also makes the vibrational lifetimes of the chalcogenides much longer than that of the ClBZN. It is interesting to note that the spectra of PhSCN and 2NPhSeCN are virtually identical. Both have a small blueshift, ~5 cm^{-1}, from PhSeCN. This blueshift for PhSCN is caused by the S replacing the Se. The blueshift for the 2NPhSeCN is caused by the bulky nitro group, which produces a change in the equilibrium orientation of the SeCN moiety by 90° relative to that of PhSeCN as discussed below when the orientational potentials are calculated.

3.2. Ultrafast Infrared Anisotropy Measurements. From eq 2, the anisotropy can be extracted from the parallel and perpendicular PSPP signals. The anisotropy decays and accompanying fits for the four probe molecules in DMF are shown in Figure 2. The anisotropy curves provided for the chalcogenides are for the center frequencies of the absorption lines (see Figure 1 and Table 1), but there is no evident frequency dependence of the anisotropy. Combination band peaks in the pump−probe spectrum of pClBZN, which arise from the coupling of the CN stretch to ring modes, grow in with the vibrational lifetime. These peaks overlap with the CN 0−1 absorption, preventing the accurate collection of the anisotropy data by measurements on the 0−1 transition.[25] Therefore, the pClBZN anisotropy data were taken on the center frequency of the 1−2 transition at 2207.7 cm^{-1}. In general, in a pump−probe experiment, measurements on the 0−1 and 1−2 transitions yield the same results. The anisotropy data for pClBZN (points) are shown in the inset of Figure 2 on a semilog plot. The line through the data is the result of a

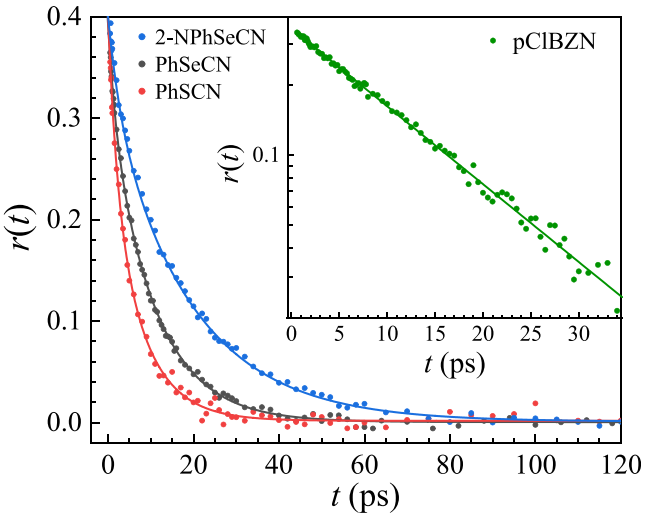

Figure 2. Anisotropy decays for the four probe molecules studied. The inset shows the anisotropy decay of *p*-chlorobenzonitrile on a semilog plot (points). The solid line through the data is the result of a single exponential fit showing that the decay is a single exponential. The main figure shows the anisotropy decays of the three probes, 2-nitrophenylselenocyanate (blue points), phenylselenocyanate (black points), and phenylthiocyanate (red points). The solid curves are fits to the WIAC model, eq 3.

single exponential fit yielding a time constant of 13.0 ± 0.1 ps with an amplitude of 0.371 ± 0.002. The single exponential for pClBZN, which has no internal bond rotation that changes the orientation of the CN transition dipole, demonstrates that DMF does not produce external physical caging. DMF has a low viscosity of 1.026 mPa s.[26] It does not form strongly associated structures that last for times long compared to 13 ps. This is in contrast to liquids such as RTILs that have strong Coulombic interactions and structuring due to interactions of alkyl moieties,[27] which result in the caging of probes such as $SeCN^-$.[8]

The anisotropy decays of PhSeCN, PhSCN, and 2NPhSeCN (points) are shown in the main part of Figure 2. These anisotropies are fit to biexponential decays (solid curves) with fit parameters given in Table 2. Testing the biexponential fits vs single exponential fits with an Akaike information criterion test showed that the biexponential fits were 10^{20} more likely to be the correct functional form than single exponential fits. As the single exponential decay data for ClBZN (inset of Figure 2) demonstrates, the biexponential decays measured for the other three probes do not arise from solvent caging causing restricted angular sampling of the entire probe molecule. The fast component of the biexponential decays of the three chalcogenide probes is caused by the internal orientational motion of the moiety containing the CN about the chalcogen-benzene bond, as shown in detail below. The range of sampling is determined by the rotational potential and the temperature rather than restrictions imposed by external physical caging.

The biexponential decays are characteristic of WIAC behavior. WIAC models the anisotropic decay as occurring in a cone with a reflecting boundary condition and fixed half angle that limits the reorientation of the probe molecule. Full randomization of the transition dipole can occur on a longer time scale by diffusive orientational relaxation of the entire molecule. With physical caging, long-time full diffusive

https://doi.org/10.1021/acs.jpcb.3c07080
J. Phys. Chem. B 2024, 128, 280−286

Table 2. Biexponential Anisotropy Decay Parameters for the Three Chalcogenides[a]

probe	t_1 (ps)	a_1	t_2 (ps)	a_2
PhSeCN	1.8 ± 0.4	0.075 ± 0.008	10.7 ± 0.2	0.317 ± 0.009
PhSCN	2.2 ± 0.3	0.16 ± 0.02	8.2 ± 0.5	0.24 ± 0.02
2NPhSeCN	3.0 ± 0.5	0.08 ± 0.008	19.2 ± 0.5	0.327 ± 0.009

[a]The t_i are the decay time constants, and the a_i are the amplitudes.

orientational relaxation requires constraint release. For limited angular sampling caused by internal rotation on a potential surface, there is no constraint release. In either case, the data can be analyzed with the WIAC formalism. WIAC analysis was performed using eq 3:[17]

$$C_2(t) = S_0^2(S_1^2 + (1 - S_1^2)\exp(-t/\tau_1))\exp(-t/\tau_D) \quad (3)$$

From the order parameters S_n, the cone half angles can be extracted according to eq 4:

$$S_i = \frac{1}{2}\cos(\theta_i)(1 + \cos(\theta_i)) \quad (4)$$

S_0 is the result of ultrafast inertial angular relaxation. The inertial decay, which is a few tens of femtoseconds, is too fast to measure. However, the value of the order parameter can be obtained by extrapolating the fit to the anisotropy decay to time zero. In eq 2, for $r(t)$, the anisotropy decay, the $t = 0$ value is 0.4. The correlation function $C(t) = 1$ at $t = 0$. So, $C(0) = 2.5r(0)$. For ClBZN, $r(0) = 0.371$, and $S_0 = 0.97$. For the other three probes, $S_0 = 1$ within error from the sum of a_1 and a_2 in Table 2. τ_D is the slow decay time constant for complete diffusive orientational relaxation. τ_1 is the fast decay constant caused by the internal orientational motion on the rotational potential surface.

Here, the zeroth and first cone angles are combined (S_0S_1) and referred to as S_{fast}. The hard cone half angles extracted from S_{fast} for PhSeCN, PhSCN, and 2NPhSeCN are 22.3 ± 1.4, 29.5 ± 9.9, and 22.2 ± 2.1°, respectively.

3.3. Wobbling in a Harmonic Cone. The results of the WIAC analysis yield the cone half angle for a hard-walled cone. In the hard cone model, molecular orientational relaxation is diffusive until the probe contacts the cone, which acts as an infinite potential barrier (reflecting boundary condition). The assumption of diffusive motion only affects the analysis of the time dependence of the probe molecules. It does not change the cone angles extracted via the order parameters. Here, we are primarily interested in the range of angles sampled. There is also a model for restricted rotational motion in which the orientational relaxation occurs on a two-dimensional angular (θ, φ) parabolic (harmonic) potential. This model is known as the harmonic cone (HC) and is given by eq 5.[19,20,28]

$$\theta_{H,Avg} = \frac{\int_0^{2\pi} d\varphi \int_0^{\pi} d\theta \sin(\theta)(\theta) e^{-I\omega^2\theta^2/2k_BT}}{\int_0^{2\pi} d\varphi \int_0^{\pi} d\theta \sin(\theta) e^{-I\omega^2\theta^2/2k_BT}} \quad (5)$$

$\theta_{H,Avg}$ is the average harmonic cone angle. It is the rotator's angle, θ, weighted by the probability of having that angle determined by the Boltzmann factor. I is the moment of inertia. ω is the harmonic oscillator frequency for the parabolic potential. k_B is the Boltzmann constant, and T is the absolute temperature. The denominator is used for probability normalization. $\theta_{H,Avg}$ is obtained by doing the angular integrations. It has been shown that for hard cone half angles of <30°, $\theta_H = \theta_O/2$, where θ_H is the harmonic cone angle and θ_O is the hard cone angle.[20] This approximation holds for all cone angles considered here.

In the three molecules studied here, the angle of the chalcogenide to the plane of the phenyl ring is sufficiently close to 90° that it can be taken as 90° without error. Below, we will briefly discuss the case where the angle is not 90° with the full details given in the SI. With θ_H known, ω is found for each molecule, and the rotational potential is generated. The parabolic potential can then act as a model for the rotational potential of the cyanate moiety with respect to the lab frame for each probe.

We have found that eq 6 is a good approximation of eq 5 at 298.15 K, but errors increase at low frequencies, small moments of inertia, and high temperatures. A simple approximation such as this shortens calculation times relative to the much more complicated eq 5.

$$\theta_{H,Avg} = \frac{5(k_BT)^{1/2}}{4I^{1/2}\omega} \quad (6)$$

Equation 5 is for molecules reorienting on a two-dimensional harmonic potential as two degrees of freedom contribute to reorientation. This applies to the reorientation of the entire probe molecule in a liquid. It has been used to determine the hydrogen bonding potential for water.[18] However, in the case of intramolecular bond rotation, only a single degree of freedom, θ, is involved. Equation 5 is therefore rewritten for one dimension, giving eq 7:

$$\theta_{H,Avg} = \frac{\int_0^{2\pi} d\theta \sin(\theta)(\theta) e^{-I\omega^2\theta^2/2k_BT}}{\int_0^{2\pi} d\theta \sin(\theta) e^{-I\omega^2\theta^2/2k_BT}} \quad (7)$$

Note that the integral is from 0 to 2π. The approximation given in eq 6 still holds for eq 7 with the same restrictions. We have found a nearly perfect numerical approximation to eq 7, i.e.,

$$\theta_{H,Avg} = \frac{1.31657 - 0.20533\omega cm^{-1}}{1 - 0.16329\omega cm^{-1}} \frac{(k_BT)^{1/2}}{I^{1/2}\omega} \quad (8)$$

Full comparisons of the numerical integral, eq 7, and the approximations, eqs 6 and 8, are given in the SI.

The wobbling in a harmonic cone model was applied to the fast WIAC decay for PhSeCN, PhSCN, and 2NPhSeCN. The cone reflects the rotational potential of the Se(S)−C−N rotating about the C−Se(S) bond. The moments of inertia for PhSeCN, PhSCN, and 2NPhSeCN were calculated using the results of DFT calculations to be 2.803×10^{-45}, 2.481×10^{-45}, and 2.797×10^{-45} kg m^2, respectively. From these, the fundamental frequencies associated with the parabolic potential (one-dimensional harmonic oscillator) can be extracted for the potential energy surface of each molecule.[18] For PhSeCN, PhSCN, and 2NPhSeCN, these are 41.2, 34.2, and 41.4 cm^{-1}, respectively.

https://doi.org/10.1021/acs.jpcb.3c07080
J. Phys. Chem. B 2024, 128, 280−286

However, these frequencies do not truly reflect the rotational potential of the cyanate moiety with respect to the phenyl ring. Because the orientational motion of the chalcogenide moiety is a vibration, the molecule as a whole cannot rotate. For the librational motion that includes rotation of the cyanate moiety, the phenyl ring counter rotates. This counter-rotation makes the angle of rotation in the molecular frame greater than in the lab frame, causing the observed potential to be steeper. To compensate for this effect, conservation of angular momentum was invoked. Then, for each probe molecule, the angular momentum of the phenyl moiety along its central axis is set equal (with the opposite sign) to the chalcogenide moiety. From this calculation, it is straightforward to determine the contribution of the phenyl rotation to the angle traversed in the molecular frame. Full detail for adding the contribution of the phenyl ring to molecular rotation is given in the Supporting Information. The new total angles for PhSeCN, PhSCN, and 2NPhSeCN are 32.23, 41.14, and 15.94°, respectively. In the molecular frame, the angles are larger than the harmonic cone angles ($\theta_O/2$, the measured cone angles divided by two). From these angles, eq 7 is once again used to calculate fundamental frequencies, which for PhSeCN, PhSCN, and 2NPhSeCN are 13.8, 11.3, and 28.7 cm^{-1}, respectively.

Comparisons between the potentials obtained from IR-PSPP anisotropy measurements with the harmonic cone model and the potentials from DFT calculations with an implicit DMF solvent are shown in Figure 3. The inset is a schematic of the

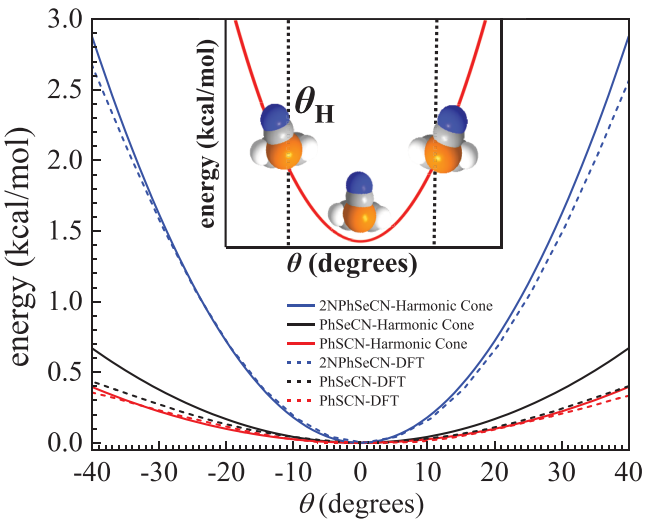

Figure 3. Comparison of potential surfaces derived from DFT calculations and the harmonic cone model. The solid lines are the harmonic cone potentials, and the dashed lines are the DFT potentials. The minimum for each potential has been set to zero degrees for the purpose of comparison. 2-Nitrophenylselenocyanate (blue), phenylselenocyanate (black), and phenylthiocyanate (red). The inset is a schematic showing a potential with a phenyl-chalcogenide at different orientations.

rotation of the chalcogen group on the potential surface. The ordering of the experimental-harmonic cone (E-HC) potentials and the DFT potentials are the same, where from shallowest to steepest the order is PhSCN, PhSeCN, and 2NPhSeCN. The E-HC and DFT potentials are very close for 2NPhSeCN. The DFT calculated full potentials for 0 to 90° are shown in Figure 4 so that the barrier heights can be seen. The 2NPhSeCN barrier is the highest at 6.6 kcal/mol. This barrier is ~11 k_BT at

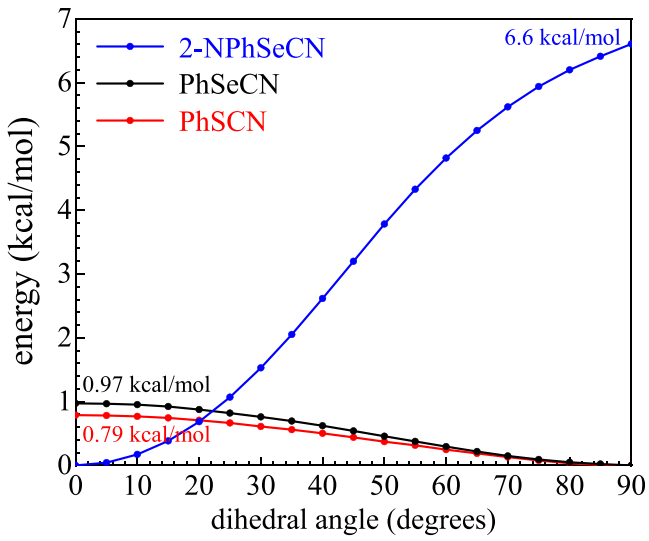

Figure 4. DFT calculations for the C(Ph)−C(Ph)−Se/S−C(CN) dihedral potential from −90 to 90° with a step size of 5° for 2-nitrophenylselenocyanate (blue), phenylselenocyanate (black), and phenylthiocyanate (red).

room temperature. Therefore, the thermally induced orientational motion of the SeCN will be near the bottom of the potential, sampling a relatively small range of angles, i.e., ~16°. Near the bottom of this steep potential, the DFT calculated potential is close to harmonic. The agreement between the E-HC and DFT potentials is quite good.

The potential barrier heights for PhSeCN and PhSCN are 0.97 and 0.79 kcal/mol, respectively (see Figure 4). These are approximately one and two-thirds and one-and-a-third k_BT at room temperature. Therefore, the angular ranges sampled for PhSeCN (~32°) and PhSCN (~42°) are much larger than for 2NPhSeCN. Because the barriers are low and the range of angles is large, the portions of the potentials sampled are less parabolic than that of 2NPhSeCN. As can be seen in Figure 3, the agreement between the E-HC and DFT calculations for PhSCN is nonetheless reasonably good. However, the comparison for PhSeCN is significantly worse. The E-HC potential is steeper than the DFT potential. This could be due to the experimental error in measuring the cone angle, θ_0. If the cone was 2° smaller, which is within the error bars, the agreement would be much better. It is also possible that the DFT with implicit solvent for PhSeCN is off to some extent. Regardless, the comparisons between the three E-HC potentials and DFT potentials are quite good and confirm the mechanism, the procedures, and the theoretical analysis of the experimental anisotropy data.

The previous theory and analysis were appropriate for the experimental results for the probes studied here, i.e., with the chalcogenide making an ~90° angle to the phenyl ring. In general, there is an additional consideration in analyzing the angle of rotation. The angle extracted from fitting to WIAC is the angle the IR chromophore makes as it depolarizes in the lab frame for the hard-walled cone. This angle is not equal to the dihedral circumscribed by the chromophore unless the bend angle relative to the remainder of the molecule is 90°. If the angle is significantly larger, the extent of depolarization is smaller than the dihedral angle circumscribed. A further effect occurs in considering the effect of a molecule going over a rotational barrier and flipping 180° along its dihedral. For the

https://doi.org/10.1021/acs.jpcb.3c07080
J. Phys. Chem. B 2024, 128, 280−286

three molecules considered in this study (chalcogenide making an ~90° angle to the phenyl ring), the probe moiety flipping 180° along its dihedral is the same as flipping 180° in the lab frame, which causes no net depolarization because the projection of the transition dipole onto the pump pulse E-field is unchanged. If, however, the bend angle is significantly different from 90°, then flipping 180° along its dihedral does result in net depolarization. The bend angle can be obtained from simple molecular structure calculations. However, the effect goes as cosine-squared of the deviation, so there is a non-negligible range of angles close to 90° for which the deviation can be neglected. A full treatment of the effects of bend angles greater than 90° is given in the SI.

4. CONCLUDING REMARKS

Ultrafast IR polarization-selective pump−probe experiments are widely used to measure the orientational relaxation of molecules in liquids and other systems. In the simplest situation, the anisotropy decay is a single exponential. The single exponential decay occurs for diffusive orientational relaxation in which all angles are sampled with a single orientational diffusion constant. An example of this behavior, the results of anisotropy measurements on *p*-chlorobenzonitrile, a single exponential decay, were presented above. However, it is not uncommon to observe biexponential decays. These decays are usually caused by the caging of the orientational probe molecule by the solvent. On a short time scale, the probe's orientational motion is constrained by the solvent change. The probe samples a limited range of angles, which is referred to as WIAC. At longer times, constraint release allows all angles to be sampled by diffusive orientational relaxation. Biexponential decays can also be expected if the probe molecules feature axes about which significantly different moments of inertia result in different time scales of diffusion, and they both affect the direction of the transition dipole being probed.

Here, we have presented another mechanism that gives rise to biexponential anisotropy decays. The fast component of the biexponential is caused by intramolecular bond rotation on a potential surface of the moiety containing the IR mode used in the experiments. In a liquid, at longer times, all angles are sampled by diffusive orientational relaxation of the entire molecule. Three molecules that display this behavior were studied with PSPP experiments. The anisotropy measurements provided the ranges of angles sampled by internal bond rotation. The range of angles is determined by the bond's rotational potential surface. The experimental data were analyzed using a one-dimensional version of the harmonic cone model. In this model, the bond rotation occurs on a one-dimensional parabolic potential. The temperature determines the extent of the angular potential that is sampled. The parabolic potentials for the three molecules were compared to the results of DFT with implicit DMF solvent calculations. For the molecule 2NPhSeCN, the agreement between the experimental results and the harmonic cone analysis, in which there are no adjustable parameters, and the DFT calculations were quite good. For this molecule, the barrier to rotation is high. The high barrier constrained the angular range to near the bottom of the potential where the shape is close to parabolic. For the other two molecules, PhSeCN and PhSCN, the agreement was only reasonable. For these two molecules, the barriers are relatively low. A wide range of angles were sampled involving regions of the potentials that deviated significantly from parabolic. The results confirm the proposed mechanism for the observed biexponential decays and the efficacy of the harmonic cone model. For moderate to steep rotational potentials, the experiment and analysis can give accurate information on the orientational potential surface.

The probe molecules studied in DMF solvent did not experience orientational caging by the solvent. For other solvents and these and other probe molecules, both internal bond rotation and intermolecular caging can occur. When both internal rotation and caging occur, several cases can arise. If the restricted range of angles by the solvent cage is smaller than the possible internal rotation range, only the solvent cage cone angle will be observed, independent of the time scale of the two processes, as the cage will block full internal orientational sampling. If the cone angle determined by the solvent cage is larger than the cone arising from internal rotation, and both types of angular sampling occur on a similar time scale, the solvent cage cone will be measured, and the first anisotropy decay, which is associated with restricted angular sampling, will likely appear as a single exponential. However, if in a liquid cage angular range is large and slow compared to internal angular sampling that is small and fast, the total restricted angular sampling will produce a biexponential decay. Following cage constraint release, there will be a third decay, i.e., diffusive sampling of all orientations. The overall decay will be triexponential.

■ ASSOCIATED CONTENT

Data Availability Statement

Data are available by contacting Professor Michael D. Fayer, Department of Chemistry, Stanford University, Stanford, CA 94305-5080, email: fayer@stanford.edu.

Supporting Information

The Supporting Information is available free of charge at https://pubs.acs.org/doi/10.1021/acs.jpcb.3c07080.

Effect of bend angles greater than 90°; comparison of exact integral and approximations (PDF)

■ AUTHOR INFORMATION

Corresponding Author

Michael D. Fayer − *Department of Chemistry, Stanford University, Stanford, California 94305, United States;* orcid.org/0000-0002-0021-1815; Phone: 650 723-4446; Email: fayer@stanford.edu

Authors

Aaron P. Charnay − *Department of Chemistry, Stanford University, Stanford, California 94305, United States;* orcid.org/0000-0003-1797-9465

Junkun Pan − *Department of Chemistry, Stanford University, Stanford, California 94305, United States;* orcid.org/0000-0001-6128-1844

Complete contact information is available at: https://pubs.acs.org/10.1021/acs.jpcb.3c07080

Author Contributions

†A.P.C. and J.P. contributed equally to this work.

Notes

The authors declare no competing financial interest.

https://doi.org/10.1021/acs.jpcb.3c07080
J. Phys. Chem. B 2024, 128, 280−286

■ ACKNOWLEDGMENTS

This work was supported by the National Science Foundation, Division of Chemistry, award number 2319637.

■ REFERENCES

(1) Brilliantov, N. V.; Denisov, V. P.; Krapivsky, P. L. Generalized Stokes-Einstein-Debye relation for charged Brownian particles in solution. *Physica A* **1991**, *175*, 293−304.
(2) Jas, G. S.; Larson, E. J.; Johnson, C. K.; Kuczera, K. Microscopic Details of Rotational Diffusion of Perylene in Organic Solvents: Molecular Dynamics Simulation and Experiment vs Debye−Stokes−Einstein Theory. *J. Phys. Chem. A* **2000**, *104*, 9841−9852.
(3) Chandler, D. Translational and rotational diffusion in liquids. II. Orientational single-particle correlation functions. *J. Chem. Phys.* **1974**, *60*, 3508−3512.
(4) McClung, R. E. D. Rotational Diffusion of Spherical-Top Molecules in Liquids. *J. Chem. Phys.* **1969**, *51*, 3842−3852.
(5) Liu, G.; Mackowiak, M.; Li, Y.; Jonas, J. Rotational diffusion of liquid toluene in confined geometry. *J. Chem. Phys.* **1991**, *94*, 239−242.
(6) Ohtori, N.; Kondo, Y.; Ishii, Y. Molecular size and shape effects: Rotational diffusion and the Stokes-Einstein-Debye relation. *J. Mol. Liq.* **2020**, *314*, No. 113764.
(7) Ishii, Y.; Murakami, T.; Ohtori, N. Molecular size and shape effects: Tracer diffusion and the Stokes-Einstein relation. *J. Mol. Liq.* **2022**, *346*, No. 118235.
(8) Breen, J. P.; Leibfried, L. C.; Xing, X.; Fayer, M. D. Long-Range Interface Effects in Room Temperature Ionic Liquids: Vibrational Lifetime Studies of Thin Films. *J. Phys. Chem. B* **2023**, *127*, 6217−6226.
(9) Roget, S. A.; Heck, T. R.; Carter-Fenk, K. A.; Fayer, M. D. Ion/Water Network Structural Dynamics in Highly Concentrated Lithium Chloride and Lithium Bromide Solutions Probed with Ultrafast Infrared Spectroscopy. *J. Phys. Chem. B* **2023**, *127*, 4532−4543.
(10) Zhang, M.; Hao, H.; Zhou, D.; Duan, Y.; Wang, Y.; Bian, H. Understanding the Microscopic Structure of a "Water-in-Salt" Lithium Ion Battery Electrolyte Probed with Ultrafast IR Spectroscopy. *J. Phys. Chem. C* **2020**, *124*, 8594−8604.
(11) Das, S.; Chakrabarty, S.; Chattopadhyay, N. Origin of Unusually High Fluorescence Anisotropy of 3-Hydroxyflavone in Water: Formation of Probe-Solvent Cage-like Cluster. *J. Phys. Chem. B* **2020**, *124*, 173−180.
(12) Lipari, G.; Szabo, A. Effect of librational motion on fluorescence depolarization and nuclear magnetic resonance relaxation in macromolecules and membranes. *Biophys. J.* **1980**, *30*, 489−506.
(13) Lipari, G.; Szabo, A. Model-free approach to the interpretation of nuclear magnetic resonance relaxation in macromolecules. 1. Theory and range of validity. *J. Am. Chem. Soc.* **1982**, *104*, 4546−4559.
(14) Fujiwara, T.; Nagayama, K. The wobbling-in-a-cone analysis of internal motion in macromolecules. *J. Chem. Phys.* **1985**, *83*, 3110−3117.
(15) Kinosita, K., Jr.; Ikegami, A.; Kawato, S. On the wobbling-in-cone analysis of fluorescence anisotropy decay. *Biophys. J.* **1982**, *37*, 461−464.
(16) Hoffman, D. J.; Fica-Contreras, S. M.; Fayer, M. D. Amorphous polymer dynamics and free volume element size distributions from ultrafast IR spectroscopy. *Proc. Natl. Acad. Sci. U.S.A.* **2020**, *117*, 13949−13958.
(17) Tan, H. S.; Piletic, I. R.; Fayer, M. D. Orientational dynamics of water confined on a nanometer length scale in reverse micelles. *J. Chem. Phys.* **2005**, *122*, 174501.
(18) Moilanen, D. E.; Fenn, E. E.; Lin, Y. S.; Skinner, J. L.; Bagchi, B.; Fayer, M. D. Water inertial reorientation: hydrogen bond strength and the angular potential. *Proc. Natl. Acad. Sci. U.S.A.* **2008**, *105*, 5295−5300.
(19) Xing, X.; Li, J.; Breen, J. P.; Karunadasa, H. I.; Fayer, M. D. Structural Dynamics of a Novel Pseudohalide Perovskite $Cs_2Pb(SeCN)_2Br_2$ Investigated with Nonlinear Infrared Spectroscopy. *J. Phys. Chem. C* **2023**, *127*, 14283−14292.
(20) Ramasesha, K.; Roberts, S. T.; Nicodemus, R. A.; Mandal, A.; Tokmakoff, A. Ultrafast 2D IR anisotropy of water reveals reorientation during hydrogen-bond switching. *J. Chem. Phys.* **2011**, *135*, No. 054509.
(21) Yan, C.; Thomaz, J. E.; Wang, Y. L.; Nishida, J.; Yuan, R.; Breen, J. P.; Fayer, M. D. Ultrafast to Ultraslow Dynamics of a Langmuir Monolayer at the Air/Water Interface Observed with Reflection Enhanced 2D IR Spectroscopy. *J. Am. Chem. Soc.* **2017**, *139*, 16518−16527.
(22) Hoffman, D. J.; Fica-Contreras, S. M.; Pan, J.; Fayer, M. D. Pulse-shaped chopping: Eliminating and characterizing heat effects in ultrafast infrared spectroscopy. *J. Chem. Phys.* **2020**, *153*, 204201.
(23) Tokmakoff, A. Orientational correlation functions and polarization selectivity for nonlinear spectroscopy of isotropic media. I. Third order. *J. Chem. Phys.* **1996**, *105*, 1−12.
(24) Tan, H.-S.; Piletic, I. R.; Fayer, M. D. Polarization selective spectroscopy experiments: methodology and pitfalls. *J. Opt. Soc. Am. B* **2005**, *22*, 2009−2017.
(25) Fica-Contreras, S. M.; Charnay, A. P.; Pan, J.; Fayer, M. D. Rethinking Vibrational Stark Spectroscopy: Peak Shifts, Line Widths, and the Role of Non-Stark Solvent Coupling. *J. Phys. Chem. B* **2023**, *127*, 717−731.
(26) Bernal-García, J. M.; Guzmán-López, A.; Cabrales-Torres, A.; Estrada-Baltazar, A.; Iglesias-Silva, G. A. Densities and Viscosities of (N,N-Dimethylformamide + Water) at Atmospheric Pressure from (283.15 to 353.15) K. *J. Chem. Eng. Data* **2008**, *53*, 1024−1027.
(27) Marsh, K. N.; Boxall, J. A.; Lichtenthaler, R. Room temperature ionic liquids and their mixtures—a review. *Fluid Ph. Equilib.* **2004**, *219*, 93−98.
(28) Kramer, P. L.; Giammanco, C. H.; Fayer, M. D. Dynamics of water, methanol, and ethanol in a room temperature ionic liquid. *J. Chem. Phys.* **2015**, *142*, 212408.

https://doi.org/10.1021/acs.jpcb.3c07080
J. Phys. Chem. B 2024, 128, 280−286